ASTRONOMY & ASTROPHYSICS
SUPPLEMENT SERIES

Astron. Astrophys. Suppl. Ser. **133**, 317–323 (1998)

Stellar kinematical data for the central region of spiral galaxies. I.⋆,⋆⋆

Ph. Héraudeau[1] **and F. Simien**[2]

[1] Max-Planck-Institut für Astronomie, Königstuhl 17, D-69117 Heidelberg, Germany
[2] CRAL-Observatoire de Lyon, CNRS: UMR 142, F-69561 St-Genis-Laval Cedex, France

Received February 26; accepted June 19, 1998

Abstract. We present the results of absorption spectroscopy on the inner region of 34 Sa-Sc galaxies. We have determined the central velocity dispersion and, for 32 of these objects, stellar rotation curves and velocity-dispersion profiles. Some of these profiles are limited to the bulge, some others do reach a region dominated by the luminosity of the disk. These data are intended to provide basic material for the study of the mass distribution and dynamical status in the central regions of spiral galaxies. Although no elaborate bulge-and-disk photometric decomposition is performed, we estimate the effects of limited resolution and contamination by disk light on the central velocity dispersion of the bulge.

Key words: galaxies: spiral — galaxies: general — galaxies: kinematics & dynamics

1. Introduction

The kinematics of the stars in the inner region of spiral galaxies can play a major role in the investigation of several key issues, a few of which are mentioned below.

To begin with, the observed motions within a bulge can be used to determine its mass and possibly its dynamical status, with the advantage (over ellipticals) that the inclination of the system is known. When the kinematics are available on a sample of bulges, they can be used to gauge, statistically, their degree of similarity with ellipticals. This can rely, for example, on the following points: a) the rotation/dispersion (V/σ_0) ratio (Kormendy 1993 and references therein); b) the $D_n - \sigma$ relation (Dressler 1987); and, c) the fundamental plane in its edge-on representation (e.g., Bender et al. 1992; Jablonka et al. 1996). Although large bulges are still thought to have been formed similarly to ellipticals, and before the disks, there is recent evidence that small bulges could have been formed later and differently (Franx 1993; Pfenniger 1993; Courteau et al. 1996); bulge kinematics provide an essential ingredient to the debate on their origin and evolution.

In a galaxy with a significant bulge, its mass is essential to the determination of the global mass distribution in the disk. Such applications often rely on a model fitted to the observed gas rotation curve (Broeils & Courteau 1997; Héraudeau & Simien 1997; Moriondo et al. 1998, to cite recent examples). But the motion of the gas in the innermost region is often an unreliable tracer of the circular rotation (Fillmore et al. 1986; Kent 1988; Bertola et al. 1995): this can strongly bias the bulge mass and, as a consequence, the disk mass as well; a way to bypass this problem is to adopt for the bulge the mass determined from the stellar kinematics.

In galaxies where the spectroscopic data extend well within the disk, one can address issues related to the old-disk dynamics (Bottema 1993). Finally, a better determination of the global stellar mass is likely to tighten the constraints on the distribution of dark matter (Bottema 1997; Courteau & Rix 1997; Persic & Salucci 1997 and references therein).

We note, however, that these applications can face several difficulties, arising from the contamination by the disk light and potential (Whitmore et al. 1984; Fillmore et al. 1986), the mixing of populations, and the effects of extinction by dust. Small bulges can be faint and difficult to resolve spectroscopically (and photometrically).

Send offprint requests to: F. Simien (simien@obs.univ-lyon1.fr)

⋆ Based on observations collected at the Observatoire de Haute-Provence.

⋆⋆ Tables 2 and 3 are presented in electronic form only; Tables 1 through 3 are available from the CDS, Strasbourg, via anonymous ftp to cdsarc.u-strasbg.fr (130.79.128.5) or via http://cdsweb.u-strasbg.fr/Abstract.html

We have run a program of absorption spectroscopy with the purpose of determining the rotation curve and the velocity-dispersion profile in a sample of spiral galaxies; we present here a first set of results.

2. Sample and observations

Our initial aim was to obtain central kinematical data on bright, nearby spirals with available surface photometry. We selected galaxies with morphological type from Sa to Sc (both unbarred and barred), intermediate inclination, $cz \lesssim 4000$ km s^{-1}, and absolute magnitude $M_B \lesssim -18$. This program has paralleled our collection of (mostly I-band) images of spiral galaxies (Héraudeau & Simien 1996: hereafter HS96); atmospheric conditions and telescope availability allowed us to get both photometric and spectroscopic data for about 50 galaxies only. Other objects were also added as targets for the spectroscopic observations because of their specific interest, regardless of the image availability. The final result is a sample which clearly lacks volume completeness and, therefore, statistical weight. It should nevertheless increase the available amount of such data significantly; in this paper, we present the first set of observations for which the reduction has been completed: 34 galaxies whose relevant catalog elements are presented in the first columns of Table 1.

Our kinematical observations were secured at the 1.93-m telescope of the Observatoire de Haute-Provence, equipped with the CARELEC long-slit spectrograph[1]. The camera aperture ratio was f/2.6, and the receptor was a Tektronix with 512×512 pixels of 27 μm, corresponding to a projected size of $1.2''$. The selected setup provided either: a) a wavelength range of ≈ 900 Å centered on Mg b, with a dispersion of 1.8 Å per pixel (corresponding to 104 km s^{-1}), or b) a range of ≈ 450 Å with a dispersion of 0.9 Å per pixel (52 km s^{-1}). The slit width, projected onto the plane of the sky, was $2.2''$.

In May and November 1992, January and February 1993, a total of 14 nights of observation allowed us to collect data on the major axis of 34 galaxies. Table 2 (in electronic form only) presents the log of the observations. Typically, two 45- or 60-minutes exposures were obtained for each object; these exposure times were short enough to prevent the widening of the spectral lines due to flexures within the spectrograph, yet long enough to allow the measurement of kinematical parameters down to surface brightnesses of $\mu_V \simeq 21$ mag arcsec^{-2}, with an accuracy for the velocity dispersion of less than 30 km s^{-1} for most objects. For NGC 2903, NGC 3675, NGC 5055, and NGC 7331, spectra along the minor axis were also obtained. Each night, several template stars of types ranging between G8III and K2III were observed.

[1] Details on the spectrograph, on the receptor, and information on the telescope itself are available on the WWW, at URL http://www.obs-hp.fr.

The atmospheric conditions were variable, with a seeing disk between $2''$ and $3''$ (FWHM) for most objects. Care has been taken to match the seeing conditions of the galaxy and star spectra, in order to ensure comparable spectroscopic resolutions.

3. Data reduction

For the reduction of the spectra, we followed closely the method used in a series of papers on early-type galaxies (Simien & Prugniel 1997a-c, 1998: hereafter collectively referred to as SP), and described in full detail in the first of these papers. We thus limit ourselves, here, to a short abstract, with emphasis on a couple of differences with respect to early-type galaxies.

Standard pre-processing was applied to the raw data, up to the rebinning in wavelength. The galaxy centers ($r = 0$) were first determined by a Gaussian fitting to a limited range ($\simeq 12''$) around the intensity peak. Compared to ellipticals, the centering was sometimes more difficult, because dust can cause strong asymmetries. In this case, and when the solution was obvious, we adopted the origin of the rotation symmetry, and we accordingly applied a correction to the r zero point. In the outer regions, cosmic-ray hits were removed with a median filter, and adjacent lines were combined with a variable weighting function (a Gaussian continuously wider faintward, up to 4 arcsec FWHM). A Fourier-Fitting technique determined the central velocity dispersion σ_0 and, when possible, the radial profile $\sigma(r)$ of the dispersion, together with the projected rotation curve $V(r)$ along the major axis. A two-pass mode (described in SP) allowed to remove cosmic rays on the inner lines, where the spatial resolution must be preserved.

The frequent presence of emission lines in the spectra of spiral galaxies makes it necessary to "cut" them at the level of the continuum; when the lines are strong, this noticeably reduces the wavelength range effectively used and, in some cases, this can contribute to lower the quality of the results.

The choice of late-type giants as template stars is particularly adapted to spectra of ellipticals and bulges; in deep spectra reaching the disk, we have not seen any evidence for a spectral mismatch: this indicates that the main disk contribution comes from the old disk.

4. Presentation of the results

Determinations of the heliocentric radial velocity $v_{\rm hel}$ and central velocity dispersion σ_0 are listed in Cols. (10) and (11) of Table 1. The $V(r)$ and $\sigma(r)$ profiles are presented in Fig. 1, and also in Table 3, which is available in electronic form only. Table 1 also lists (Col. 12) a factor $f_{\rm bulge}$

Table 1. Catalog elements and spectroscopic results

Object	Type	α_{1950}	δ_{1950}	$B_{\rm Tc}$	D_{25}	ϵ_{25}	PA	$-M_B$	$v_{\rm hel}$	σ_0	$f_{\rm bulge}$
(1)	(2)	(3)	(4)	(5)	(6)	(7)	(8)	(9)	(10)	(11)	(12)
NGC 772	Sb	01 56 35.3	+18 45 49	10.27	7.5	0.42	130	22.36	2453 ±14	143 ±13	1.02
NGC 1024	Sab	02 36 30.4	+10 37 55	12.27	3.5	0.63	155	21.11	3512 ±38	168 ±18	1.04
NGC 1169	SBb	03 00 11.5	+46 11 21	10.63	4.4	0.41	28	22.03	2394 ±16	150 ±25	1.05
NGC 1589	Sab	04 28 11.2	+00 45 24	11.67	3.2	0.69	160	21.81	3765 ±39	199 ±18	1.03
NGC 2146	SBab	06 10 42.7	+78 22 23	10.32	5.6	0.43	123	20.59	884 ±30	125 ±35	1.03
NGC 2336	SBbc	07 18 28.0	+80 16 35	10.12	6.7	0.43	178	22.45	2189 ±11	120 ±11	1.06
NGC 2633	SBb	08 42 35.7	+74 16 59	12.15	2.3	0.37	175	20.38	2166 ±15	100 ±29	1.07
NGC 2648	Sa	08 39 53.3	+14 27 57	12.02	3.3	0.59	148	20.17	2006 ±20	162 ±13	1.06
NGC 2712	SBb	08 56 09.7	+45 06 38	12.06	2.9	0.46	178	20.03	1838 ±17	97 ±15	1.03
NGC 2742	Sc	09 03 38.6	+60 40 51	11.25	3.0	0.49	87	20.24	1303 ±16	68 ±30	1.00
NGC 2841	Sb	09 18 34.9	+51 11 18	9.22	7.7	0.53	147	20.95	629 ±15	198 ±13	1.03
NGC 2894	Sa	09 26 50.6	+07 56 13	12.57	1.9	0.50	27	19.68	2112 ±18	155 ±22	....
NGC 2903	SBbc	09 29 19.9	+21 43 18	8.69	12.1	0.54	17	20.82	558 ±13	101 ±13	0.96
NGC 2916	Sb	09 32 07.6	+21 55 45	12.19	2.5	0.33	20	21.32	3668 ±15	139 ±14	1.00
NGC 2964	SBbc	09 39 56.4	+32 04 35	11.23	3.0	0.43	97	20.15	1328 ±12	97 ±19	....
NGC 3031	Sb	09 51 27.6	+69 18 12	6.95	24.3	0.51	157	21.48	-25 ±12	166 ±12	1.00
NGC 3169	Sa	10 11 38.7	+03 43 02	10.56	4.5	0.44	45	20.46	1266 ±17	171 ±17	1.05
NGC 3190	Sa	10 15 20.2	+22 05 00	11.31	4.3	0.58	125	20.00	1271 ±14	169 ±11	1.03
NGC 3254	Sbc	10 26 31.3	+29 44 49	11.37	4.8	0.69	46	20.02	1371 ±14	115 ±18	1.08
NGC 3627	SBb	11 17 37.9	+13 16 08	8.77	9.1	0.55	173	21.25	742 ±15	117 ±09	....
NGC 3675	Sb	11 23 24.2	+43 51 36	10.38	6.2	0.43	178	20.09	751 ±13	121 ±05	1.03
NGC 3718	SBa	11 29 50.7	+53 20 32	10.89	7.4	0.44	15	20.14	1011 ±23	178 ±19	0.92
NGC 3726	SBc	11 30 38.3	+47 18 12	10.27	6.0	0.32	10	20.49	846 ±12	73 ±26	1.05
NGC 4258	SBbc	12 16 29.7	+47 34 54	8.01	17.5	0.62	150	21.02	480 ±09	115 ±10	1.00
NGC 4303	SBbc	12 19 21.4	+04 44 57	9.75	6.5	0.09	162	21.88	1569 ±17	74 ±09	....
NGC 4501	Sb	12 29 28.1	+14 41 49	9.46	6.8	0.46	140	23.01	2268 ±12	151 ±17	1.05
NGC 4579	SBb	12 35 12.6	+12 05 39	9.93	5.9	0.20	95	21.67	1507 ±12	127 ±17	....
NGC 4826	Sab	12 54 16.9	+21 57 17	8.46	10.3	0.51	115	20.56	393 ±14	113 ±13	1.04
NGC 5033	Sc	13 11 09.7	+36 51 29	9.66	9.9	0.62	170	21.07	891 ±12	138 ±10	1.04
NGC 5055	Sbc	13 13 34.9	+42 17 54	8.56	13.0	0.40	105	21.27	486 ±10	117 ±07	1.02
NGC 6643	Sc	18 21 13.2	+74 32 43	10.59	4.4	0.51	38	21.28	1492 ±19	75 ±24	0.95
NGC 7331	Sbc	22 34 47.7	+34 09 34	9.06	10.6	0.59	171	21.60	814 ±07	139 ±06	1.03
NGC 7448	Sbc	22 57 34.9	+15 42 50	11.27	2.6	0.55	170	21.17	2179 ±22	57 ±15	0.91
UGC 3828	SBb	07 20 21.5	+58 04 00	12.65	1.7	0.46	0	20.66	3484 ±19	102 ±25	1.03

Notes. Cols. (2) to (9) are from the LEDA database (status: LEDA1998); Cols. (10) to (12) are determinations of this work. Col. (2): morphological type; cols. (3), (4): coordinates; Col. (5): $B_{\rm Tc}$, integrated blue magnitude, corrected for Galactic and internal extinction; Col. (6): D_{25}, diameter at isophote $\mu_B = 25$ mag arcsec^{-2}, in arcmin; Col. (7): ϵ_{25}, ellipticity at isophote $\mu_B = 25$; Col. (8): PA, position angle of major axis, in degrees (North through East); Col. (9): M_B, absolute B magnitude, from $B_{\rm Tc}$ and kinematical distance modulus with $H_0 = 75\,{\rm km\,s^{-1}\,Mpc^{-1}}$, except for objects with a very small radial velocity (for which LEDA makes use of other parameters); Col. (10): $v_{\rm hel}$, heliocentric radial velocity, in km s^{-1}; Col. (11): σ_0, central velocity dispersion, in km s^{-1}; Col. (12): $f_{\rm bulge}$, factor indicating the degree to which resolution effects and contamination by disk light have influenced the observed central bulge kinematics; $\sigma_0/f_{\rm bulge}$ is then a closer approximation to the averaged, luminosity weighted bulge velocity dispersion within $0.1r_{\rm e}$ (see Sect. 5 and the Appendix).

measuring the effects of resolution and disk-light contamination on the central velocity dispersion of the bulge; this is discussed in the Appendix below.

As in SP, we have adopted the following convention for the position angle PA: for $0 < {\rm PA} < 180°$, $r < 0$ corresponds to the eastern side of the galaxy, for $180 < {\rm PA} < 360°$, $r < 0$ corresponds to the western side, and for ${\rm PA} = 0°$, $r < 0$ is to the North.

Table 1, Table 2, and Table 3 are available from the CDS. The data presented here, including the graphs of Fig. 1, are also available at the HYPERCAT on-line catalog browser (Prugniel et al. 1998), at the following URL: http://www-obs.univ-lyon1.fr/hypercat/.

5. Discussion

We have determined the central velocity dispersion in 34 spiral galaxies. For 32 of them, we have presented profiles of the projected rotation velocity and velocity dispersion, along at least one main axis. Our data significantly

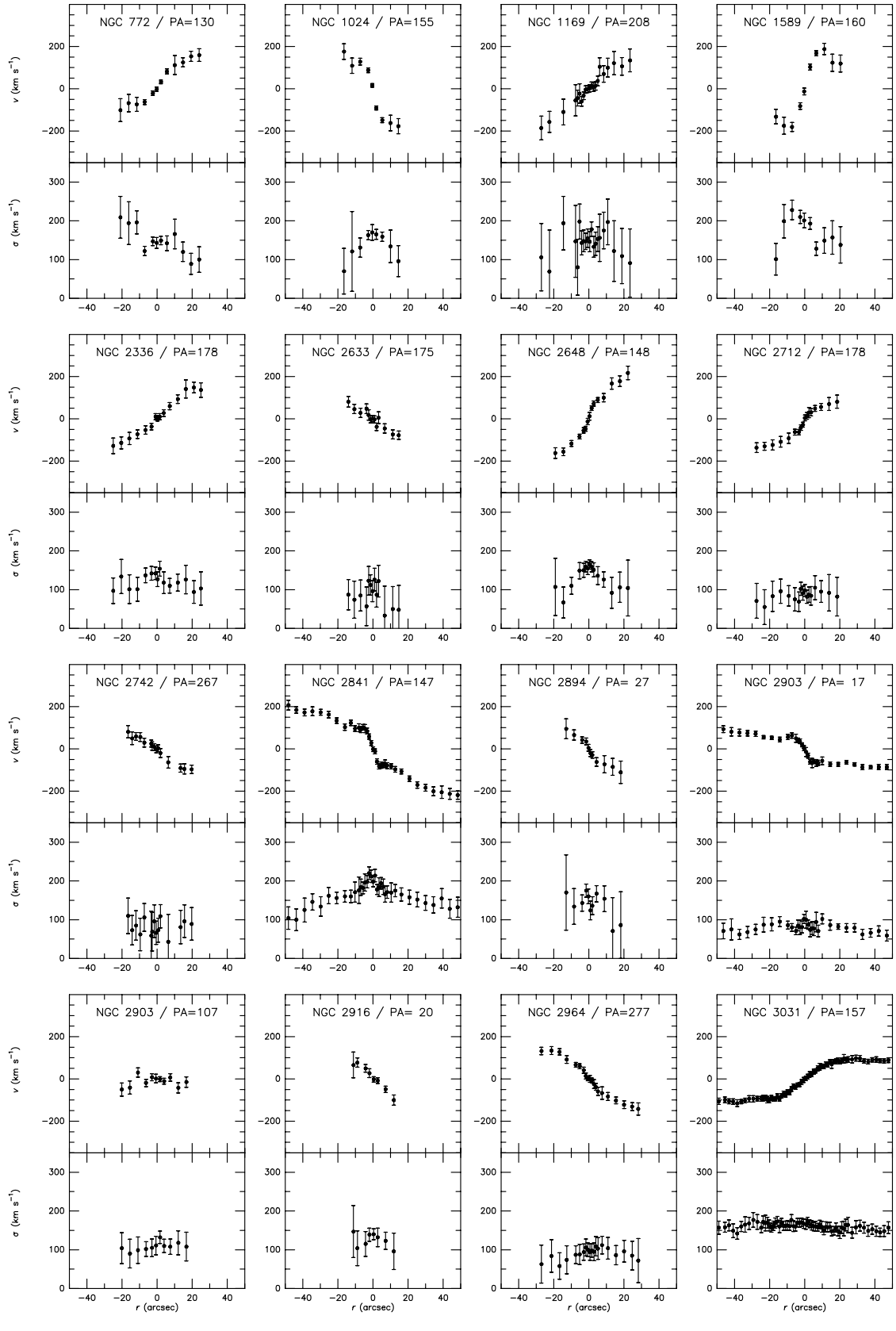

Fig. 1. Profiles of rotation velocities and velocity dispersions

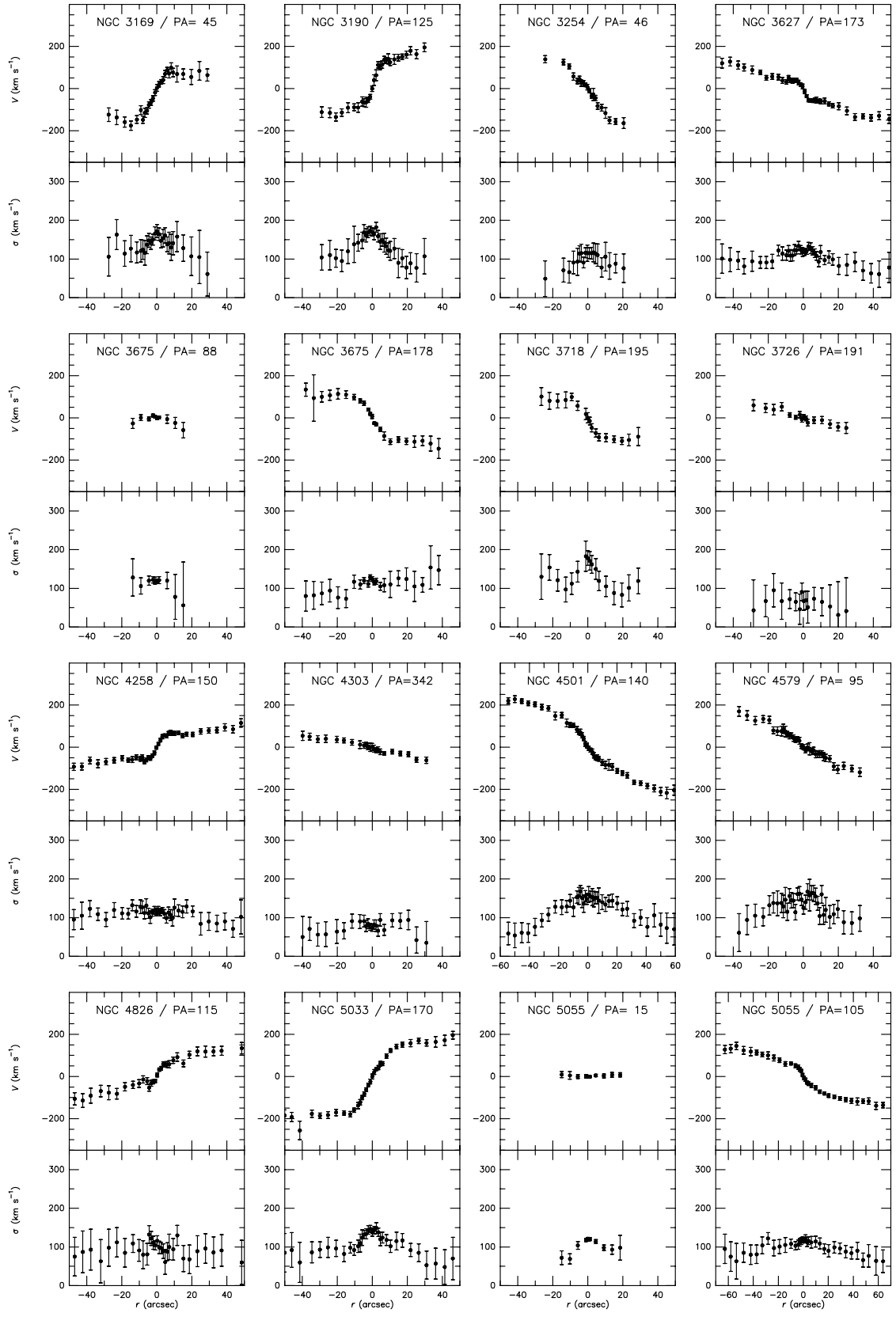

Fig. 1. continued

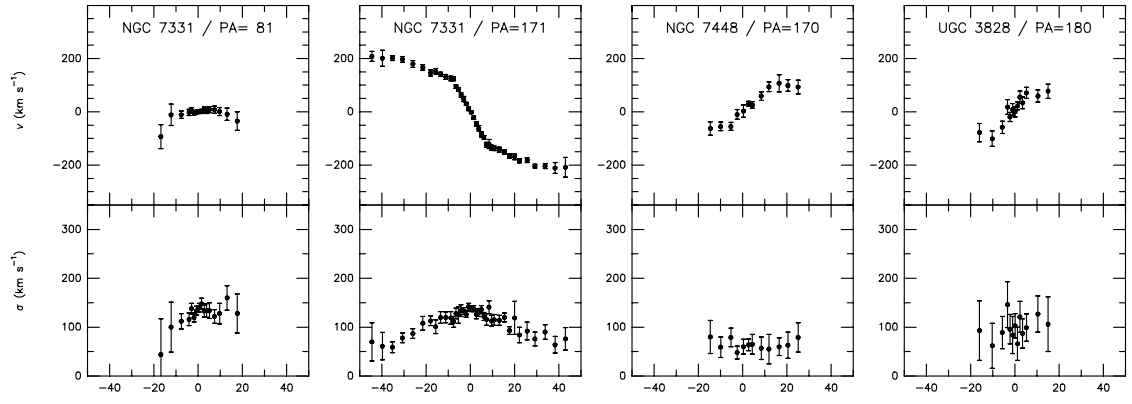

Fig. 1. continued

increase the very limited amount already available in the literature: the compilations of McElroy (1995) and Prugniel & Simien (1996) indicate that the central velocity dispersion was so far published for 16 of these objects, and a rotation curve for only nine.

At variance with SP, we have not listed in Table 1 a maximum velocity of rotation $V_{\rm max}$. Knowledge of the maximum rotation velocity of the central bulge would be valuable as a constraint on its mass and dynamical status, but the influence of the disk is (in most cases) important, and even when a conspicuous inner "plateau" is visible in the rotation curve, it cannot be connected to the bulge $V_{\rm max}$ in a dependable way. As for the disk maximum rotation, few of our spectra are deep enough to determine it (a small but significant difference with the gas rotation should be present).

Although applications to both bulges and disks can be considered, the present data are clearly biased toward the formers. It is thus relevant to ask the following question: How is σ_0 related to the kinematics of the bulge population? The answer is not straightforward, and several aspects of the problem have to be detailed, as below.

To begin with, a typical bulge is a fast rotator, compared to bright ellipticals; for our observations at intermediate or high inclination, at the very center, resolution effects (integration due to pixel and slit dimensions, atmospheric smearing) tend to widen the apparent line-of-sight velocity distribution (the LOSVD), thus increasing σ_0. The light from the colder disk, when superimposed on the bulge in sufficient quantity, has the opposite effect on σ_0. The resulting balance can be accurately determined if: a) a bulge+disk photometric decomposition is performed, b) a dynamical model is applied and integrated along the line of sight, and c) comparison to the observations is made with proper attention to the fact that the LOSVD of the model is likely non-Gaussian, since the two components, locally, show different rotational velocities as well as velocity dispersions.

This has recently been applied, for example, to edge-on S0 galaxies (Loyer et al. 1998), and this elaborate modeling is beyond the scope of the present paper. Instead, we have limited ourselves to a simpler estimate of the resolution and disk-contamination effects on the central bulge kinematics (see Appendix); as a result, we list in Col. (12) of Table 1 a factor $f_{\rm bulge}$ by which the bulge velocity dispersion, averaged within a tenth of its effective radius ($0.1r_{\rm e}$), has been modified to give the observed σ_0. We note that $f_{\rm bulge}$ is close to unity, and that the correction is, for most bulges, marginal compared to the error bars of the present data.

We now stress two more points: first, although $\sigma_0/f_{\rm bulge}$ is intended to represent a physical kinematical parameter, it scales only a part of the total kinetic energy; from Binney (1978), and Prugniel & Simien (1994), we can estimate to $\simeq 20\%$ the ratio of the rotational to the random kinetic energy for bulges of spiral galaxies. Second, detailed individual models can be significantly complicated by a barred or triaxial geometry; for most of these galaxies, isophote parameters can be found in HS96 for a previous check.

We will present in the near future similar data for a complementary sample of more recent observations, together with comparisons to other sources (Héraudeau & Simien, in preparation); we also plan to study relevant correlations and detailed kinematical modeling.

Acknowledgements. We are endebted to the telescope operators at the Observatoire de Haute-Provence for their help in collecting the data. We thank an anonymous referee for valuable comments on previous versions of the manuscript. We have made use of the Lyon-Meudon Extragalactic Database operated by the LEDA team.

Appendix. Resolution effects and bulge+disk luminosity mixing

The elements needed for the calculations are the following: a) the respective bulge and disk surface brightnesses; b) their rotation velocities and velocity dispersions; and, c) an estimate of the seeing conditions during the spectroscopic observations. Although an elaborate bulge+disk photometric decomposition was not

attempted in the present work, we have been able to set boundaries to the range of possible values for the parameters involved, so that relevant simulations could be performed.

We consider an oblate bulge with a $r^{1/n}$ luminosity law (Sérsic 1968). Although intrinsically bright bulges are well represented by a de Vaucouleurs law ($n = 4$), small ones are better fit by exponential ($n = 1$) models (Andredakis et al. 1995; Courteau et al. 1996). For the disk, we have assumed that, in the region most affected by resolution effects, its brightness is constant. For each galaxy, this value was estimated on the HS96 V-band photometric profile by extrapolating toward the center the exponential region of the disk; a correction was applied when there was evidence of a "type II" profile (Freeman 1970). The apparent bulge central brightness was determined on the same photometric profile, after a crude correction to the same seeing conditions as for the spectroscopic observations. Let $\delta_{\rm mag}$ be the apparent, central magnitude difference betweeen the bulge and disk components; $\delta_{\rm mag}$, n and the effective radius $r_{\rm e}$ of the bulge fully determine the photometric structure needed for our calculations. $\delta_{\rm mag}$ is quite easy to determine; we found values from 1 to more than 3 mag arcsec^{-2}, with an average of 2.4 and a rms scatter of 0.7. But n and $r_{\rm e}$ are more complicated to determine, and we limited ourselves to the definition of the following range of values; for n: between 1 and 4; for $r_{\rm e}$: between a couple of arcsecs and an upper value leading to a profile obviously too bright in the disk region.

For the bulge, a dynamical model similar to that of Prugniel & Simien (1997) has been used, solving the Jeans equations for a $r^{1/n}$ density law; in the present work, we included an intrinsic flattening ($\epsilon = 0.3$ on average), and this resulted into a mean rotation curve determined by the assumed isotropy of the residual velocities. The rotation of the disk has been neglected at the center. For its velocity dispersion, we have adopted a central value connected to that of the bulge: from the data of Bottema (1993), we estimated that $\sigma_{\rm disk}/\sigma_{\rm bulge} = 0.5$ for galaxies with a high bulge-to-disk ratio ($\delta_{\rm mag} > 2$ mag arcsec^{-2}), and $\sigma_{\rm disk}/\sigma_{\rm bulge} = 0.7$ for galaxies with a smaller bulge.

For each galaxy, after setting the above parameters, we started with $\sigma_{\rm in}$, the velocity dispersion for the bulge model, averaged within $0.1r_{\rm e}$, and we calculated the resulting disk-contaminated, projected, convolved and rebinned central velocity dispersion $\sigma_{\rm out}$; the calculation was made with different values of $r_{\rm e}$ and n, and we have adopted for $f_{\rm bulge}$ the average value of the ratio $\sigma_{\rm out}/\sigma_{\rm in}$; the scatter of this ratio reflects the sensitivity to the parameter values; the typical uncertainty on $f_{\rm bulge}$ is ± 0.04.

References

Andredakis Y.C., Peletier R.F., Balcells M., 1995, MNRAS 275, 874
Bender R., Burstein D., Faber S.M., 1992, ApJ 399, 462
Binney J., 1978, MNRAS 183, 501
Bottema R., 1993, A&A 275, 16
Bottema R., 1997, A&A 328, 517
Bertola F., Cinzano P., Corsini E.M., 1995, ApJ 448, L13
Broeils A.H., Courteau S., 1997, in: Dark and visible matter in galaxies, Salucci P., Persic M. (eds.), PASPC 117, 74
Courteau S., de Jong R.F., Broeils A.H., 1996, ApJ 457, L73
Courteau S., Rix H.-W., 1997, in: Galactic halos, Zaritsky D. (ed.), PASPC 136, 196
Dressler A., 1987, ApJ 317, 1
Fillmore J.A., Boroson T.A., Dressler A., 1986, ApJ 302, 208
Franx M., 1993, in: Galactic bulges, Dejonghe H., Habing H.J. (eds.). Kluwer (Dordrecht), p. 243
Freeman K.C., 1970, ApJ 160, 811
Héraudeau Ph., Simien F., 1996, A&AS 118, 111 (HS96)
Héraudeau Ph., Simien F., 1997, A&A 326, 897
Jablonka P., Martin P., Arimoto N., 1996, AJ 112, 1415
Kent S.M., 1988, AJ 96, 514
Kormendy J., 1993, in: Galactic bulges, Dejonghe H., Habing H.J. (eds.) Kluwer (Dordrecht), p. 209
Loyer E., Simien F., Michard R., Prugniel Ph., 1998, A&A 334, 805
McElroy D.B., 1995, ApJS 100, 105
Moriondo G., Giovanardi C., Hunt L.K., 1998, A&A (in press)
Persic M., Salucci P., 1997, in: Dark and visible matter in galaxies, Salucci P., Persic M. (eds.), PASPC 117, 1
Pfenniger D., 1993, in: Galactic bulges, Dejonghe H., Habing H.J. (eds.), Kluwer (Dordrecht), p. 387
Prugniel Ph., Simien F., 1994, A&A 282, L1
Prugniel Ph., Simien F., 1996, A&A 309, 749
Prugniel Ph., Simien F., 1997, A&A 321, 111
Prugniel Ph., Zasov A., Busarello G., Simien F., 1998, A&AS 127, 117
Sérsic J.-L., 1968, AJ 73, 892
Simien F., Prugniel Ph., 1997a, A&AS 122, 521
Simien F., Prugniel Ph., 1997b, A&AS 126, 15
Simien F., Prugniel Ph., 1997c, A&AS 126, 519
Simien F., Prugniel Ph., 1998, A&AS 131, 287
Whitmore B.C., Rubin V.C., Kent Ford Jr. W., 1984, ApJ 287, 66